metals

MDPI

Review

A Review of Multi-Scale Computational Modeling Tools for Predicting Structures and Properties of Multi-Principal Element Alloys

Mohsen Beyramali Kivy [1], Yu Hong [2] and Mohsen Asle Zaeem [2,*]

[1] Materials Engineering Department, California Polytechnic State University, 1 Grand Ave, San Luis Obispo, CA 93407, USA; mbeyrama@calpoly.edu

[2] Mechanical Engineering Department, 1610 Illinois St., Colorado School of Mines, Golden, CO 80401, USA; yuhong@mines.edu

* Correspondence: zaeem@mines.edu

Received: 14 January 2019; Accepted: 9 February 2019; Published: 20 February 2019

Abstract: Multi-principal element (MPE) alloys can be designed to have outstanding properties for a variety of applications. However, because of the compositional and phase complexity of these alloys, the experimental efforts in this area have often utilized trial and error tests. Consequently, computational modeling and simulations have emerged as power tools to accelerate the study and design of MPE alloys while decreasing the experimental costs. In this article, various computational modeling tools (such as density functional theory calculations and atomistic simulations) used to study the nano/microstructures and properties (such as mechanical and magnetic properties) of MPE alloys are reviewed. The advantages and limitations of these computational tools are also discussed. This study aims to assist the researchers to identify the capabilities of the state-of-the-art computational modeling and simulations for MPE alloy research.

Keywords: multi-principal element alloys; computational models; first-principles calculations; molecular dynamics; phases; properties

1. Introduction

Multi-principal element (MPE) alloys, are a specific class of multicomponent alloys consisted of five or more alloying elements usually with near equi-atomic compositions [1]. The development of MPE alloys can be retrospect to one and a half decades ago, opening the door to alloy design with a vast variety of compositions, microstructures and properties [2]. Since then, numerous research projects have been conducted regarding the design, development, and study of different aspects of these alloys. However, the majority of these studies have been done using experiments involving trials and errors [3]. Due to the different type of principal elements in MPE alloys, designing of these alloys to achieve desired microstructures and properties is a challenging task. In addition to the severe lattice distortions and very sluggish elemental diffusions due to different neighboring atomic sites in each lattice [4,5], cocktail effects and high order of elemental interactions make designing of these alloys difficult [1]. In traditional design of MPE alloys only substitutional elements were considered, and the latest designs of MPE alloys that consider interstitial elements or precipitants [6–10] have increased the design intricacy of these alloys. Fundamental studies on phase formations, microstructure evolutions, and structural transformations of these alloys are required.

Figure 1 shows how the number of publications on MPE alloys has dramatically increased over the years since the first publications in 2004. The data used in Figure 1 is extracted from the Scopus abstract and citation database in December 2018, using high entropy alloy and/or multi principal

element alloy keywords. Based on this data, more than 2300 research articles have been published in various journals and a number of publications are growing remarkably every year.

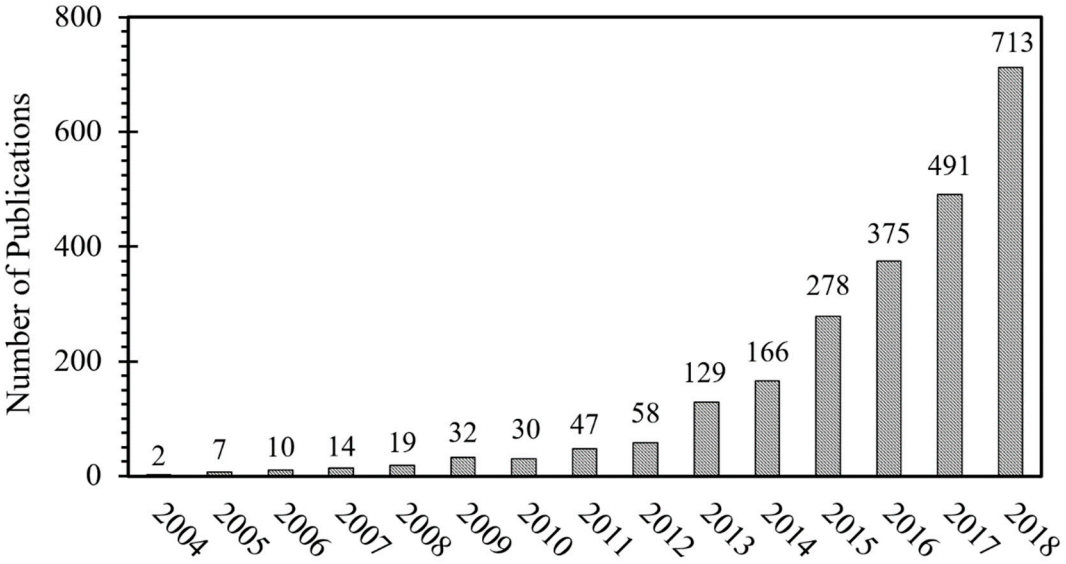

Figure 1. Number of publications on multi-principal element (MPE) alloys per year.

According to the comprehensive review article of Miracle and Senkov [1] in 2017, 37 different elements have been used so far to produce MPE alloys. These elements were 22 transition metals, six lanthanides, three metalloids, two basic metals, two alkaline earth metals, one alkali metal, and one non-metal [1]. Figure 2 shows the most common elements used in MPE alloys [1] with their value rates and price fluctuations (volatility) over 10 years period [11]. As it can be seen, most of these common elements are low-priced elements, however elements with intermediate prices (e.g., Co) or even high price (e.g., Ta) are used to produce MPE alloys as well.

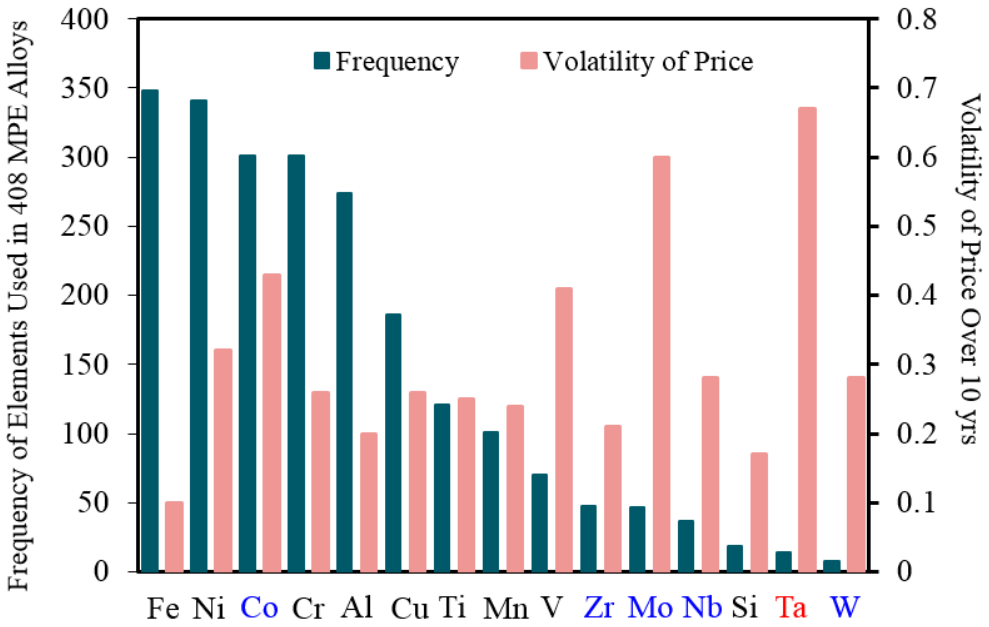

Figure 2. The most common elements used in MPE alloys [1] and their volatility of prices over a period of 10 years. Black elements have a low price (~$0.5/mole of average 50 years), blue elements have an intermediate price (~$5/mole of average 50 years), and the red element has a high price (~$100/mole of average 50 years) [11].

Traditionally, the term high entropy alloys (HEAs) have been employed broadly by researchers to describe the MPE alloys. This high entropy definition is based on the ideal configurational molar entropy, calculable by Boltzmann equation [12]. Based on this definition, metallic alloys with $\Delta S_{config}^{ideal} \geq 1.61R$ (where R is gas constant) are called HEAs. The primary problem with this description is that it denotes a single value of configurational entropy for each alloy system [1]. This assumption can be viable if the atomic positions on lattices are totally random. However, alloy configurational entropy can constantly change with temperature due to the change in atomic positions, formation of different phases, elemental segregations, and possible phase transformations [1,13]. Another approach to defining MPE alloys that have been used in the literature is compositional-based definition instead of the entropy-based concept. In this approach, these alloys are called complex concentrated alloys (CCAs). Based on this definition, alloys with non equi-molar compositions, and/or alloys with four alloying elements are also considered as CCAs [1].

Figure 3 illustrates the relationship between the properties/price ratio and the entropy of common alloys [14]. According to this data, MPE alloys (HEAs in this figure) can be expensive (medium to low cost effective), but some of them may belong to the most cost-effective zone which includes metallic glasses and super alloys, and further research is needed for their design and development [14]. It should be mentioned that the authors in Figure 3 have employed the ideal configurational entropy. Therefore, considering the complexity of configurational entropy of MPE alloys as a function of composition, atomic configuration, and temperature, the projected property-price relationship and its variation with alloy entropy can change.

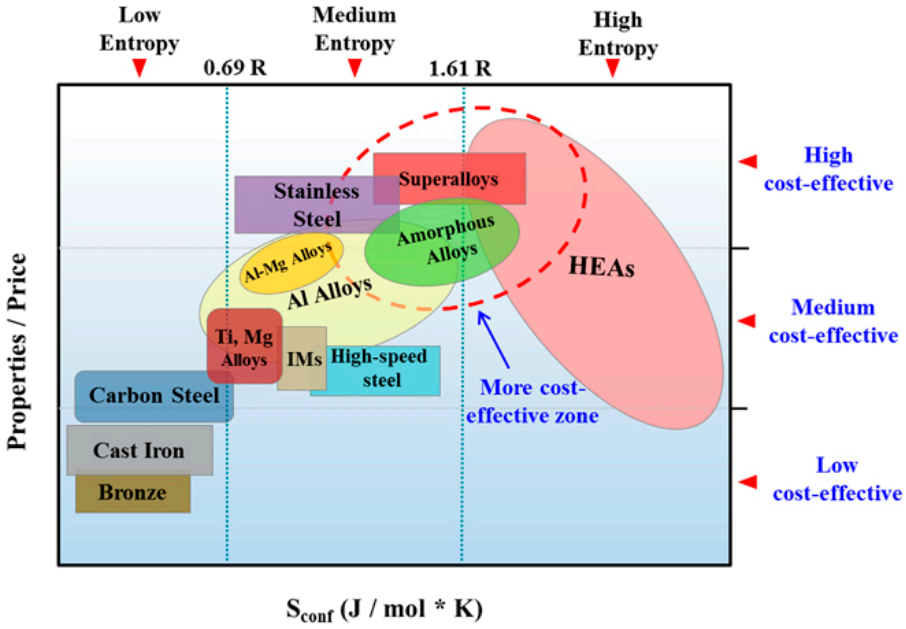

Figure 3. Relationship between property/price ratio and the configurational entropy of common alloys (this figure is from Reference [14]; IMs: Intermetallics or metallic compounds).

To overcome the complexities in experimental design of MPE alloys, reduce the inevitable expenses in empirical investigations, and decrease the number of time-consuming trials and errors, developing and utilizing computational modeling and simulations seem to be credible. Over the years various computational modeling tools have been developed or utilized in order to predict the microstructures and properties of different MPE alloys. In this study, we review the research articles published in the last decade studying different features of the MPE alloys by using computational modeling and simulations. This study is prepared in two major sections. First, the studies on phase equilibria and crystal structures of the MPE alloys are discussed, and then the research about predicting the properties of the MPE alloys are reviewed. Furthermore, in each section and shortcomings of each

of the computational modeling tools are clarified. The purpose of this review article is to provide the current state of the art in computational modeling and simulations of MPE alloys, and assist the researchers to gain more knowledge about their capabilities and shortcomings in the study and design of these alloys.

2. Phase Equilibria and Crystal Structures of MPE Alloys

Similar to other alloy systems, nano- and microstructures of MPE alloys essentially affect their properties. In spite of being compositionally complex due to having multiple principal elements, the majority of MPE alloys are designed to form simple microstructures, mainly solid solutions (SS) [15]. Miracle and Senkov [1] reported that from 643 different studied MPE alloys, SS microstructures were the most common with 48% of all the cases. SS plus intermetallics (IM) microstructures are 42%, and IM microstructures are only 10%. Moreover, within the reported SS microstructures for various MPE alloys under different processing conditions (e.g., as-cast, heat treated, etc.), single-phase SS is the most common SS microstructure (25% of the cases) and double-phase SS ranks second (17%). Body-centered cubic (bcc) and face-centered cubic (fcc) phases are the most common phases in the experimentally studied MPE alloys (43% and 56%, respectively), while MPE alloys with an hcp phase are very rare (1%) [1]. Therefore, regardless of thermodynamic stabilities/instabilities of these reported microstructures discussed by E.J. Pickering and N.G. Jones [16], the strong tendency to form simple microstructures could make it easy to theoretically predict the microstructures and investigate the phase equilibria of MPE alloys. On the other hand, the presence of multiple principal elements increases the order of interactions between the elements which can result in the complexity of calculations and computational simulations.

Calculating the phase equilibria, predicting the stable phases and crystal structures, and investigating the phase formations/transformations are the initial steps in computational materials design. Over the last few years various computational techniques and theoretical approaches have been utilized to study and predict the phase equilibria and crystal structures of MPE alloys. These theoretical and computational studies provide valuable information about the various aspects of the crystal structures and microstructure evolutions of MPE alloys, however, they have their limitations and challenges.

Zhang et al. study on the relationship between SS stability, atomic size difference (δ), and enthalpy of mixing (ΔH_{mix}) was one of the earliest theoretical studies attempted to predict the crystal structures and phases of MPE alloys [17]. According to their study, SS in MPE alloys forms when $1 \leq \delta \leq 6$ satisfying Hume-Rothery rule [18], and $-15kJ.mol^{-1} \leq \Delta H_{mix} \leq 15kJ.mol^{-1}$ [17]. Figure 4 shows how SS and ordered SS microstructures in MPE alloys can be achieved when $1 \leq \delta \leq 6$ and $-15kJ.mol^{-1} \leq \Delta H_{mix} \leq 5kJ.mol^{-1}$ [17].

Later, Guo et al. [19] reported a successful study about the relationship between valance electron concentration (VEC) and crystal structures of the MPE alloys. Their study suggested that a single bcc phase forms for $VEC < 6.87$, while for $VEC \geq 8$, a single fcc phase is stabilized. Consequently at $6.87 \leq VEC < 8$, both fcc and bcc phases can co-exist in the microstructure of an MPE alloy [19]. The VEC criterion has been also applied to determine the presence of σ-phase in Cr and V containing MPE alloys [20]. According to Tsai et al. [20], σ-phase can be stabilized in Cr and V containing MPE alloys if $6.88 \leq VEC \leq 7.84$. These criteria have been applied to many different MPE alloys and the results seem to be mostly consistent with experiment [21].

Thermodynamics based approaches are some of the most popular techniques that can be applied to theoretically study the phase equilibria of materials without laborious and rather expensive experiments. Various thermodynamic methods and approaches are available to study different characteristics of alloys, including MPE alloys. For instance, Ye et al. [13] studied the trend of the elemental segregation in the number of SS MPE alloys by calculating the deviation of a designed composition from the optimum composition at different temperatures using their modified thermodynamic regular solution model [13]. In another example, Morral and Chen [22] studied the

miscibility gaps and their stabilities in MPE alloys using thermodynamical criteria. Furthermore, the semi-empirical calculation of phase diagram (CALPHAD) method, which method is based on minimization of the free energy of the system, was introduced in 1970 by Kaufman and Bernstein [23,24]. CALPHAD method is known to be the most general and extensible method capable of predicting the phase equilibria of MPE alloy systems [25].

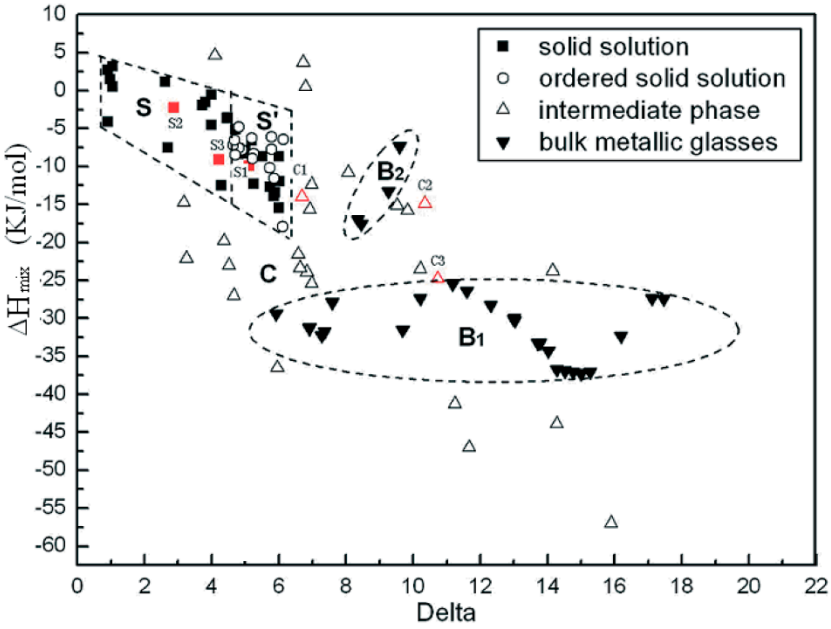

Figure 4. Microstructures of MPE alloys and Bulk Metallic Glasses as a function of enthalpy of mixing and atomic size difference (this figure is from Reference [17]).

It has been shown that in multicomponent systems, three separate Gibbs free energies can be considered to determine the total Gibbs free energy of a phase (Equation (1)) [25]:

$$G^{Phase} = G^0 + G^{ideal} + G^{excess}, \quad (1)$$

where G^0 is the reference Gibbs energy equivalent to the mechanical mixture of the constitute components of the phase, G^{ideal} is the ideal Gibbs energy corresponding to the ideal solution entropy of mixing, and G^{excess} is the excess Gibbs energy for a regular solution.

CALPHAD method is available in some thermodynamic software packages, such as Factsage [26], Thermo-Calc [27,28], and Pandat [29]. In addition to predicting structures and phases of MPE alloys, thermodynamic methods were also used to calculate the mixing enthalpy, configurational entropy, mismatch entropy, and other thermodynamic aspects of high entropy bulk metallic glasses (HE-BMGs) [30,31].

Thermo-Calc has recently become arguably the best commercial tool to study the phase equilibria of multicomponent systems, including MPE alloys. For example, Tang et al. [32] were able to determine the stabilities of different Al-transition metal binary phases in some MPE alloys by calculating their enthalpy of mixing using the Thermo-Calc SSOL5 database. Sonkusare et al. [33] calculated sudo-binary phase diagram of CoCuFeMnNi, Saal et al. [34] studied the phase fractions of CoCrFeMnAl, Yao et al. [35] computed the mixing Gibbs free energies and phase fraction of four refractory MPE alloys, Fang et al. [36] determined the phase molar fractions of selected light-weight MPE alloys, and Stepanov et al. [37] calculated the phase molar fractions of $AlCr_xNbTiV$, using TCHEA1, TCHEA2, TCNI7, TCNI8, and TTTI3 databases of Thermo-Calc, respectively. Moreover, B. Gwalani et al. [38] have comprehensively studied the effects of thermo-mechanical processes on microstructures of $Al_{0.3}$CoCrFeNi MPE alloy and their discrepancies from thermodynamic predictions

by TCHEA database of Thermo-Calc. According to this study, nanoscale ordered $L1_2$ phase was formed experimentally when the alloy was solutionized at 1150 °C before annealing. This meta-stable $L1_2$ phase was not captured in the equilibrium thermodynamic calculations due to different driving forces for nucleation, as well as different nucleation barriers in different phases [38]. According to the recent comprehensive study of Abu-Odeh et al. [39], the calculated phase equilibria of 71% of alloys (153 alloys out of 216 total studied alloys) using TCHEA1 (the database deigned for MPE alloys) matched the experiments. In another study, Tancret et al. [40] have reported the predictive capability of TCNI7, TTNI8, TCFE8, and SSOL5 databases of Thermo-Calc. According to this study, TCFE8 was the most successful database for MPE alloys, while SSOL5 was the most accurate for non-MPE alloys [40]. Figure 5 shows the accuracy of different CALPHAD databases in predicting the phase formations in MPE and non-MPE alloys [41]. It should be noted that current databases of Thermo-Calc are not able to capture the phase formations in most of the experimentally studied MPE alloys.

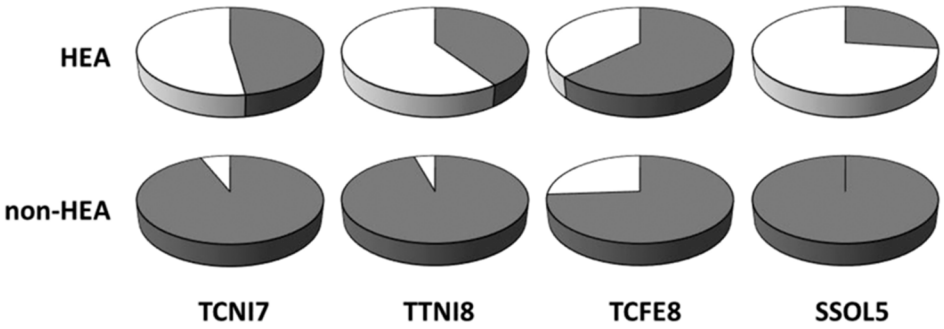

Figure 5. Capability of four different CALPHAD databases in predicting the formation of MPE alloys (HEA) and others (non-HEA). Dark sectors show success and light sectors represent the failure of the data bases (this figure is from Reference [41]).

The Pandat thermodynamic software package has also been utilized to study the phase equilibria of a few MPE alloys. For instance, Liu et al. [42] calculated the phase molar fractions and a phase diagram of $AlCrCuFeNi_2$ alloys using the PanHEA database of Pandat. Nevertheless, some researchers prefer to develop their own thermodynamic databases [43,44] or use the available CALPHAD-based databases (e.g., SGTE) directly without using commercial software [45,46]. This will allow these frameworks to study MPE alloys for which there are not enough experimental data available in the databases of commercial software. A statistical study was performed by Miracle and Senkov [1] illustrating the predictive capability of the CALPHAD calculations with respect to the experimental results. They compared two CALPHAD datasets (f_{AB} = 1 and f_{AB} = All) at two different temperatures (600 °C and melting temperature (T_m)). According to their findings, CALPHAD predicts more phases in the microstructures of the MPE alloys than the experimental observations. Also, some phases are over predicted while some phases are neglected. In addition to predicting structures and phases of MPE alloys, thermodynamic methods and approaches were also used to calculate the mixing enthalpy, configurational entropy, mismatch entropy, and other thermodynamic aspects of high entropy bulk metallic glasses (HE-BMGs) [30,31].

First-principles approaches (electronic scale simulations), including density functional theory (DFT) calculations and ab-initio molecular dynamics (AIMD) simulations, are other strong theoretical tools which can provide the thermodynamic information and phase stabilities of MPE alloys with good precisions. These approaches are the smallest scale simulations in the multi-scale computational materials framework and are known to be the most successful methods to study the electronic structures of materials [47]. Different commercial and open-access ab-initio based software packages, such as VASP [48], Quantum Espresso [49], ABINIT [50], and CASTEP [51], are available to study different aspects of the MPE alloys. First-principles approaches have been used to study the phase equilibria and crystal structures of different MPE alloys. For instance, Ma et al. [52] studied

the thermodynamic properties of the CoCrFeMnNi using DFT and AIMD. They found that the ferromagnetic hcp structure is stable at ground state with respect to other structures (bcc or fcc) and other magnetic states (non-magnetic or disordered local moments). They also calculated the temperature dependent free energy values of different crystal structures and magnetic states, and temperature dependent vibrational entropy, magnetic entropy, and electronic entropy [52]. In other examples, Niu et al. [53] calculated the mixing enthalpy and lattice constant of NiFeCrCo, Yalamanchili et al. [54] studied the configurational entropy of (AlTiVNbCr)N, Jiang and Uberuaga [55] developed an ab-initio based small set of ordered structures (SSOS) and calculated the instability energies as energy difference between fcc and bcc structures for different bcc MPE alloys, Tian et al. [56] studied the similar energy difference for number of CoMoW-based MPE alloys, Li et al. [57] calculated the hcp-fcc energy difference, lattice vibration, and magnetic entropy of $Co_{20}Cr_{20}Fe_{40-x}Mn_{20}Ni_x$ MPE alloys, Heidelmann et al. [58] determined the stable structures for matrix and inter-grain phases of ZrNbTiTaHf, and Mu et al. [59] computed the lattice constants of five different refractory MPE alloys, all using first-principles calculations.

Moreover, first-principles approaches can provide information about phase evolutions and structural properties of the MPE alloys. For example, Zhang et al. [60] determined an unstable sluggish pressure-induced phase transformation from fcc to hcp in NiCoCrFe alloy by calculating the Gibbs free energies and lattice constants of fcc and hcp phases at different pressures and lattice volumes. In another study, Tian et al. [61] investigated the phase stabilities of paramagnetic $(NiCoFeCr)_{1-y}Al_y$ MPE alloys by calculating Gibbs free energies and structural energies of different phases as a function of Al content, Middleburgh et al. [62] studied the segregation and migration of species in CrCoFeNi alloys by calculating the vacancy energy and defect energy versus lattice binding energies, Yu et al. [63] investigated the nano-scale phase separation in some fcc MPE alloys using ground state formation energies, and Leong et al. [64] applied the rigid band approximation (RBA), a simplification of density functional theory approach, to investigate the phase formation behaviors in MPE alloys and several phases were successfully predicted.

In addition to crystal structures and phase formations, other nano/microstructure and phase equilibria related properties can be calculated using first-principles approaches. For example, Gutierrez et al. [65] calculated the melting temperature, chemical energy, and specific heat of CoCrFeNiMn MPE alloys. They also calculated the temperature dependent thermal expansion and lattice constants. Due to the complexity of the MPE alloys with high chemical disorder and composition fluctuation, energy dissipation and defect evolution have also been important topics to study, especially for designing radiation resistant materials used in extreme radiation environments. Based on first-principles approaches, Y. Zhang et al. [66] applied ab initio Korringa–Kohn–Rostoker coherent-potential-approximation (KKR-CPA) method for electron structure calculations of NiCoFeCr to study the controlling factors in radiation resistance mechanisms. Based on their first-principles and experiments, they suggested that exploiting single-phase concentrated solid solutions of MPEs could be an effective approach to modifying intrinsic material transport properties, which can affect equilibrium and non-equilibrium defect dynamics [66].

First-principles calculations can also be integrated with thermodynamic CALPHAD models to study the phase stabilities and phase diagrams of MPE alloys. For instance, enthalpy of mixing for different structures and compositions can be calculated using DFT methods and the results can be considered in the CALPHAD formulations [67,68]. The advantage of incorporating first principles with CALPHAD approaches is to improve the predictive capabilities of CALPHAD by adding more physical factors into the calculations [69].

Despite the capabilities of the first-principles approaches in studying the structures and phase equilibria of the MPE alloys [70], small scale (pm to nm), small number of atoms (a few hundred atoms), and relatively high computational costs are the main limitations of these methods. Therefore, using combinations of thermodynamics and first-principles approaches have shown better promising results in studying the MPE alloys [71–73].

In addition to the first-principles and thermodynamics approaches as the most popular methods to study the crystal structures and phase equilibria of MPE alloys, other multi-scale computational methods, such as molecular dynamics (MD), Monte-Carlo, and some analytical-numerical methods have also been applied to study different features of the microstructures of some MPE alloys. For instance, Choi et al. [74] studied the migration vacancy energies of the species in CoCrFeMnNi alloy, and Sharma et al. [75] calculated the crystallization temperatures and stable phases in $Al_XCrCoFeNi$ alloy, using MD simulations with considering second nearest-neighbor modified embedded atom method (2NN-MEAM) and Lennard-Jones (LJ) potentials, respectively. The main problem in using the MD simulations is generally the unavailability of the interatomic potentials. If the interatomic potentials are not specifically developed for the target materials or the temperature of interest, the results may not be useful or accurate. Developing interatomic potentials can be a time-consuming and computationally expensive process.

Some researchers have utilized Monte Carlo simulations which are a broad range of computerized mathematical algorithms to study the probability of different objectives [76]. For example, Anzorena et al. [77] investigated the evolution probabilities with temperature for different coordination matrices in MoTaVWZr, and Feng et al. [78] calculated the pair correlation functions in AlCoCrFeNi; both work employed Monte Carlo simulations. In another work, hybrid Monte Carlo and MD (hybrid MC/MD) approach was used to simulate the structure and calculate the partial radial distribution functions in $Al_{1.33}$CoCrFeNi MPE alloy (Figure 6) [79]. The large amounts of the required data in Monte Carlo simulations usually increase the complexity of such simulations.

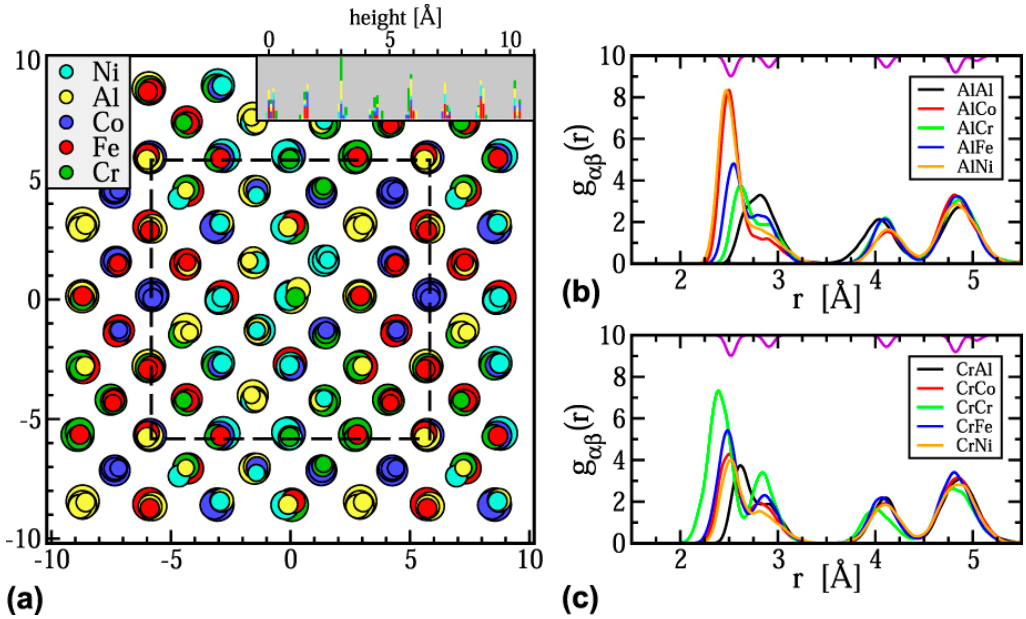

Figure 6. (**a**) Simulated structure of $Al_{1.33}$CoCrFeNi at T = 300 K viewed along the [001] direction. (**b**) and (**c**) Partial radial distribution functions $g_{\alpha\beta}(r)$ showing the atomic distributions around Al and Cr atoms, respectively (this figure is from Reference [79]).

It should be noted that some characteristics and properties of the MPE alloys have been studied by other numerical, analytical, and statistical analyses, such as lattice distortion by an analytical calculation method [80], lattice constants and short range order matrices by a theoretical atomistic model [81], densities and melting temperatures by a combination of physical and statistical models [82], and elemental diffusivities by combinations of different theoretical methods, including Darken and Miedema's scheme [83].

Although the reviewed multi-scale computational tools improve the research capabilities in study and design MPE alloys, due to the configurational disorders in MPE alloys, these approaches still have

uncertainties and errors, either in modeling or calculations. Various models have been utilized in the literature to study the structures and properties of different systems. For instance, coherent potential approximation (CPA) to study the chemical and magnetic disorders, special quasi-random structure (SQS) as one of the most successful models known for binary and ternary alloys, and coarse-grain cluster expansion (CE) to investigate short-range order effects in Monte-Carlo simulations [55]. In two recent studies, Fernandez-Caballero et al. [84,85] investigated the configurational entropy as a functional temperature, and calculated the multi-body ordering probabilities and short range ordering (SRO) for Cr-Fe-Mn-Ni and MNbTaVW MPE systems, by developing a hybrid combinations of effective cluster interactions (ECIs) derived from DFT and Semi-Canonical Monte Carlo Simulations.

Due to the unique characteristics of MPE alloys, such as a large number of alloying elements, high interaction order, and large local atomic displacements (lattice distortions), there are some noticeable discrepancies between computational data and experiments [55]. The uncertainty of computational data must be reported, which is often ignored, and more efforts need to be dedicated to developing more accurate models.

3. Properties of MPE Alloys

3.1. Mechanical Properties

MPE alloys can be designed to have exceptional mechanical properties. As it can be seen in Figure 7 [86], MPE alloys can show excellent damage tolerance (strength combined with toughness) when compared to conventional alloys. Therefore, a more comprehensive understanding of the mechanical behaviors of MPE alloys can result in optimization the design of these alloys.

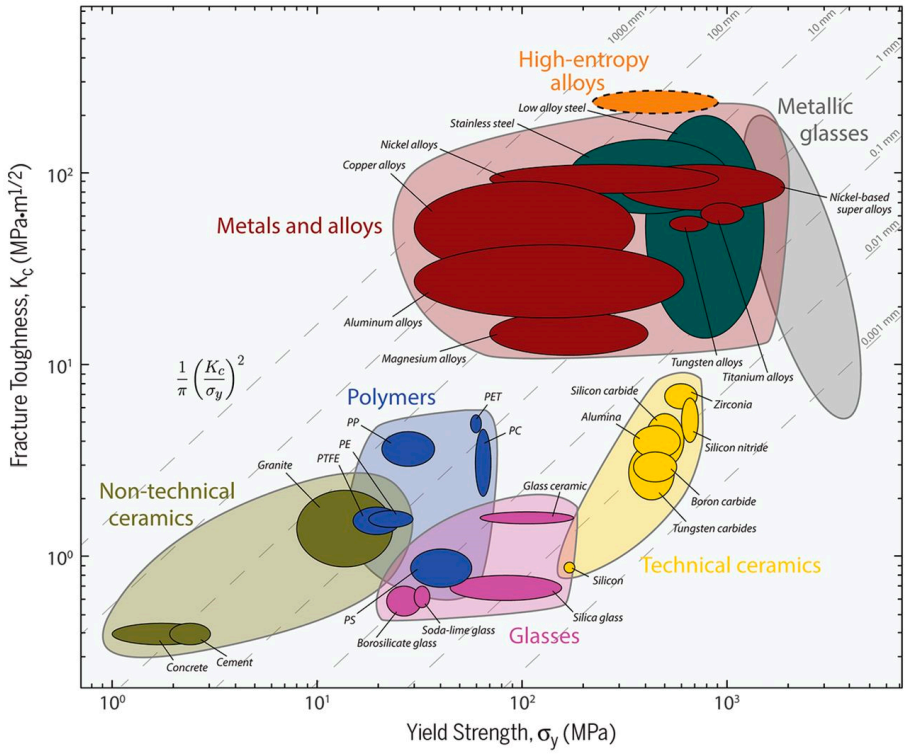

Figure 7. Fracture toughness as a function of yield strength for a wide variety of materials, including MPE alloys (high entropy alloys) (this figure is from Reference [86]).

Generally, elastic constants (C), bulk modulus (B), Young's modulus (E), shear modulus (G), and the Poisson ratio (υ) are some of the most important mechanical properties of alloys. To measure the elastic constants through experimental technique, large and homogeneous single crystal samples

without any defects are required. As a result, limited experimental data on the elastic constants of MPE alloys have been reported in the literature. Due to the great challenges of experimental studies in this area, computational modeling tools have become essential alternatives to study the properties of MPE alloys in a time-efficient and low-cost manner. In the following subsections, different mechanical properties of MPE alloys predicted by computational approaches are reviewed.

3.1.1. Elastic Properties

Elastic properties are determined by applying external forces bellow the yield limit on computer models.

Starting with first-principles calculations at the electronic scale, exact muffin-tin orbital (EMTO) method [87] is an efficient approach to solve Kohn–Sham equations, while coherent potential approximation (CPA) [88] is a technique which can powerfully treat the substitutional disorder for degrees of freedom of chemical and magnetic. It was demonstrated that combined EMTO and CPA (EMTO-CPA) can successfully predict the elastic properties of materials. For example, Tian et al. [89] employed the EMTO-CPA method to determine the elastic properties and equilibrium volume of CoCrFeMnNi based MPE alloys. They also studied the effects of alloying elements on electronic structures and elastic properties of $TiZrNbMoV_x$ MPE alloys [90]. Moreover, they indicated that the VEC value of about 4.72 is critical for the elastic isotropy in these refractory MPE alloys. In another study, Li et al. [91] utilized first-principles calculations to determine the effects of crystallographic directions on the Young's modulus of some fcc and hcp MPE alloys (see Figure 8).

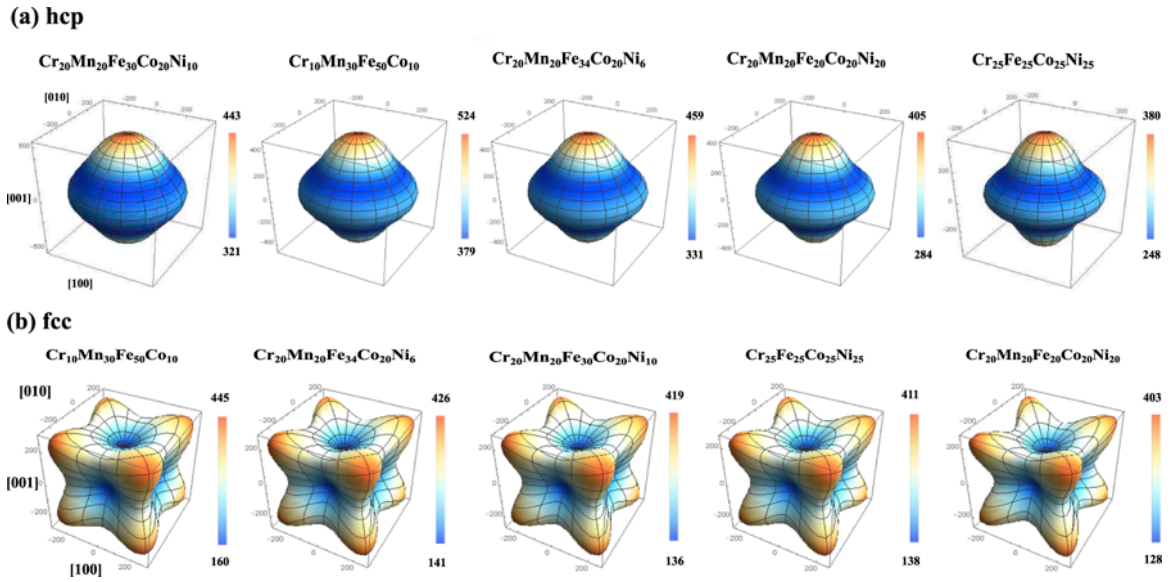

Figure 8. Directional dependence of Young's modulus E (in GPa) of some MPE alloys in hcp and fcc structures (this figure is from Reference [91]).

In another first-principles study, Cao et al. [92] investigated the equilibrium bulk properties of $Al_xMoNbTiV$ alloys by employing EMTO-CPA, in which the fraction of Al was controlled between x = 0 and x = 1.5. They have shown that the υ, B/G ratio and ab-initio Cauchy pressure of these alloys decreased with the increase of Al content. Moreover, these alloys were predicted to become isotropic when VEC ≈ 4.82 or x ≈ 0.4. Employing the EMTO-CPA method, Li et al. [93] studied the equilibrium volume, the ideal tensile strength, and elastic properties of some bcc-phase MPE alloys, ZrVTiNb, ZrNbHf, ZrVTiNbHf and ZrTiNbHf. The obtained results were expected to provide a guideline to design refractory MPE alloys with controlled strength level [93]. Furthermore, Li et al. [94] investigated the variation behaviors of the ideal tensile strength (ITS) and the ideal shear strength (ISS) in terms of the composition of elements. The ab-initio EMTO-CPA calculations were combined with the

quasi-harmonic Debye-Grüneisen model by Ge et al. [95] to investigate the equilibrium bulk properties, thermo-elastic properties, and the Curie temperature of ferromagnetic and paramagnetic CoCrFeMnNi alloys. In their study, the elastic moduli were found to linearly decrease and the ductility increase with the temperature increase [95]. All of these studies demonstrated that integrated the EMTO-CPA method is capable of determining elastic properties of MPE alloys with five or fewer elements.

Virtual lattice approximation (VCA) is a method that allows the study of a crystal structure that its primitive unit cell can be periodically repeated, but it contains fictitious "virtual" atoms that interrupt between the atoms behaviors in the parent material [96]. By combining DFT and VCA methods, Tian et al. [97] calculated the elastic constants, ITS and ISS of single-phase TiVNbMo alloys. Their simulation results implied that the single-phase bcc TiVNbMo exhibits good ductility, but low tensile strength and shear strength [97]. Moreover, Mu et al. [59] used ab-initio EMTO and VCA methods to study the properties of refractory MPE alloys. They showed that the refractory MPE alloys consisting of Cr, Ti, Ta, Zr, V, Mo, Nb and W have stable single-phase bcc instead of fcc and hcp phases [59]. Also their studied alloys showed superior ductile and isotropic properties [59].

Table 1 summarizes the available Young's moduli of various MPE alloys in the literature. Despite the great progress that has been achieved by the aforementioned computational approaches, great amounts of experimental studies are still needed to validate the obtained computational results.

Table 1. Available Young's moduli (GPa) of MPE alloys in literature.

Alloys	E_{DFT}	E_{MD}	$E_{exp.}$
$Al_{0.1}CoCrFeNi$	-	199 [99]	203 [99]
CoCrFeNi	275.7 [94], 274.1 [89], 225 [100], 196 [100]	-	226 [101]
CoCrMnNi	265.6 [89]	-	171 [100]
CoFeMnNi	267.2 [95]	-	-
CoCrFeMnNi	262.4 [94], 279.7 [95], 207 [100]	-	215 [102], 137 [100]
$Cr_{10}Mn_{40}Fe_{40}Co_{10}$	328.1 [94]	-	-
TiZrVMoTaNb	71.9 [59]	-	-
TiZrVMoTaNbCr	130.9 [59]	-	-
TiZrVMoTaNbCrW	166.7 [59]	-	-
NbVTiZrAl	118.0 [98]	-	-
ZrNbHf	95.4 [93]	-	-
ZrVTiNb	95.1 [98], 117.5 [93]	-	80 [103], 101 [104]
ZrTiNbHf	88.9 [93]	-	-
ZrVTiNbHf	97.1 [93]	-	-
$TiZrNbMoV_x$	141.1 (x = 1) [90], 127.8 [96]	-	-
$Al_xMoNbTiV$	174.4 (x = 1) [92], 185.4 [96]	-	-
TaNbHfZrTi	185.4 [96]	-	78.5 [103], 87 [104]
NbTaTiWV	257.3 [96]	-	-
WNbMoTaV	218.0 [96]	-	-
MoNbTaTiV	130.5 [96]	-	-
MoTiZrNbHfTa	136.6 [96]	-	-

In addition to EMTO-CPA and VCA methods, several other theories and methods were developed to predict elastic properties of MPE alloys. The maximum entropy (MaxEnt) method [96], which is based on the first-principles, is used to study the effect of lattice distortions on the elasticity of several single-phase MPE alloys. Compared to EMTO-CPA, it has been shown that MaxEnt is a more reliable method in studying the elastic properties of MPE alloys, as well as studying the local atomic environment [96]. Moreover, the MaxEnt method can be potentially used in the MPE alloy systems with 4 to 10 elements, with different concentrations [96]. In addition to the discussed methods, first-principles approaches can be directly applied to study the mechanical properties of MPE alloys. For instance, Qiu et al. [98] examined the effect of Al on structure stability, electronic structure, chemical bonding and mechanical properties, such as strengthening mechanisms of bcc NbVTiZrAl alloys by directly using first-principles calculations.

Although, the majority of the studies on elastic properties of MPE alloys have used first-principles based approaches, some meso-scale computational techniques also have sparsely employed. For example, a finite element analysis (FEA) model was developed by Štamborsk et al. [105] to study the effect of anisotropic as-cast microstructure on high-temperature compression deformation of multiphase $Co_{24}Cr_{19}Fe_{24}Ni_{19}Al_8(Ti,Si,C)_6$ Compositionally Complex Alloys (CCA), which is derived from single phase CoCrFeNi-based MPE alloys. They qualitatively studied the local microstructure evolutions, such as the fragmentation of brittle phase and plastic deformation of the ductile phases, with respect to 3D numerical modelling of local strains and stresses [105]. Their approach was proposed to be helpful in the initial screening of the composition of alloy during the design of new MPE alloys [105].

3.1.2. Plastic Deformation

Similar to the other types of structural material, it is essential to study the plastic deformation behaviors and the underlying deformation mechanisms of MPE alloys [106].

In a study on equimolar MPE alloys, Ye et al. [107] identified a non-symmetric residual strain field using first-principles calculations with atomic scale fluctuations, which provided a further understanding of the plasticity enhancement in MPE alloys, such as dislocation strengthening. Besides, to calculate the essential residual strain in MPE alloys and other types of alloys, Ye et al. [108] developed a self-sufficient geometric model. This approach is expected to be useful in compositional selection for designing of new MPE alloys. But the chemistry effects were ignored in their calculations [108].

The stacking fault energy (SFE) of materials is one of the most important factors in determining the dominant plastic deformation mechanisms. By using a first-principles approach, Kivy and Asle Zaeem [109] recently calculated the generalized stacking fault energy (GSFE) of CoCrFeNi-based single phase MPE alloys to investigate the effect of Cu, Ti, Mo, Mn, Al elements on their plastic deformation mechanisms. With randomly distributed alloy systems, possible variations in formation energies were obtained. Uncertainties were calculated by first running five to nine simulations for each composition to determine the atomic positions within the DFT supercell that results in the most stable (lowest energy) configuration, then, the stacking fault plane was placed at different locations to take into account the composition effects at the stacking fault plane and its neighboring planes on GSFE calculations. Examples of calculating GSFE curves are shown in Figure 9. This study demonstrated that relatively high amounts of Al, or the presence of Cu and Mn, endorse martensitic transformation and dislocation mediated slip as plastic deformation mechanisms. Alternatively, mechanical twining and dislocation glide in alloys containing Mo or Ti, and dislocation gliding for alloys with a low amount of Al would be the plastic deformation mechanisms [109].

In another study, SFEs for a series of solid solution alloys (SSAs) were studied by first-principles calculations [110]. Their obtained results indicated that these SSAs exhibit low (even negative) SFEs depending on the alloying elements [110]. To determine the temperature dependence of the SFE in Fe-Cr-Co-Ni-Mn alloy, Huang et al. [111] analyzed the chemical, strain and magnetic effects using the first-principles method. They predicted very low SFE values with a large positive temperature factor at cryogenic conditions, which can be used to explain the observed twinning induced plasticity (TWIP) effect at temperatures lower than zero and transformation induced plasticity (TRIP) effect. These effects may also explain the observed combinations of superior ductility and strength of Fe-Cr-Co-Ni-Mn MPE alloys [111].

With a different approach, Pei et al. [112] used the algorithm of particle swarm optimization within Peierls–Nabarro model to obtain the dislocation structures and provided a pathway to efficiently determine their mobility and geometries.

In a recent study, Choudhuri et al. [113] investigated the effects of σ and B2 intermetallic phases on deformation twinning of $Al_{0.3}$CoCrFeN MPE alloy, using a combination of experiments and MD simulations. According to this study, σ and B2 intermetallic compounds endorsed deformation twining and strain hardening of the fcc matrix. They used ~900 K atoms with an EAM interatomic potential in

their simulations [113]. In a three dimensional MD simulation study, Wang et al. [114] investigated the strengthening mechanism and plastic deformation behaviors of AlCrCuFeNi MPE alloys. They used 1.5 M atom simulations utilizing a combination of EAM and Morse potential, and determined the surface topography, friction coefficient, dislocation density and subsurface damaged structure during the process of nanoscale scratching, and the dynamic evolution of scratching forces, and compared them with those in pure metals [114]. In another study, the strain-induced transformation plasticity of single-crystal and nanocrystalline $Co_{25}Ni_{25}Fe_{25}Al_{7.5}Cu_{17.5}$ MPE alloy during fcc to bcc phase transition was investigated using MD simulations by Li et al. [115]. With 2.3M atom simulations using a normalized EAM potential, they concluded that the fcc to bcc phase transition provides an alternative approach in designing novel MPE alloys with improved strength and ductility [115]. Sharma and Balasubramanian [99] have investigated the deformation mechanisms of a single phase $Al_{0.1}$CoCrFeNi, under tension by employing MD simulations. They considered an EAM-LJ hybrid potential with 62,500 atoms. Their simulation results attempted to offer insights on the nucleation and dynamic evolution of defects, which cannot be achieved by experiments and not unfeasible by first-principles calculations [99]. Finally, by employing MD simulations focusing on dislocation motion behavior, and utilizing an EAM potential in 1.4M atom simulations, Smith et al. [116] demonstrated that the SFE in equiatomic CrMnFeCoNi MPE alloys should be considered as a spatially local property instead of global variable. In Table 2 the calculated SFE values of several MPE alloys by DFT, MD, and experiment are compared, demonstrating that calculations of SFE is mostly ignored by the most of previous MD studies, therefore one can't confidently utilize such MD simulations to study plastic deformation in MPE alloys.

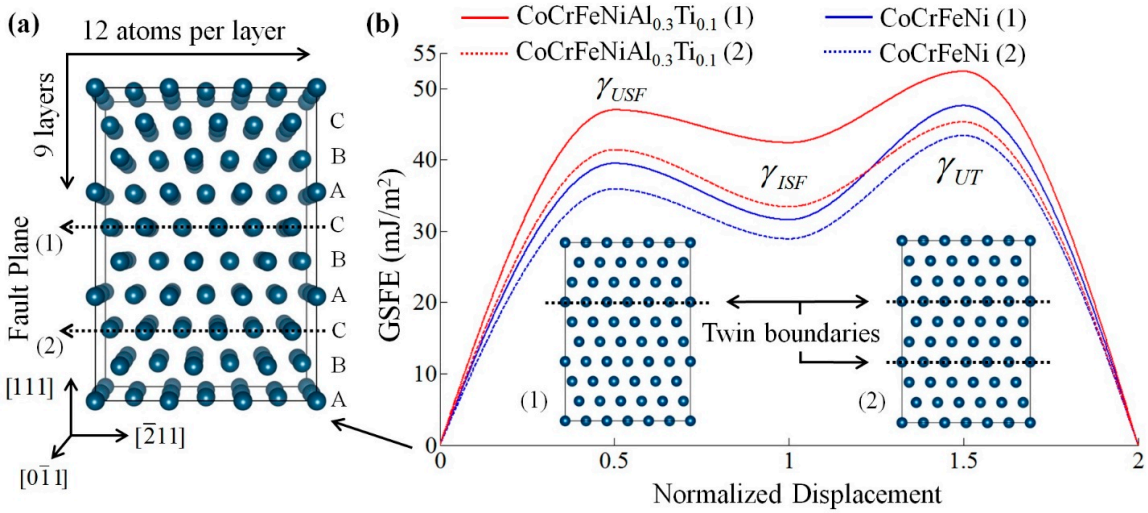

Figure 9. (**a**) fcc supercell structure used for calculating generalized stacking fault energy curves and surface energies of CoCrFeNi-based single phase MPE alloys. (**b**) Calculated GSFE curves for CoCrFeNi and CoCrFeNiAl0.3Ti0.1 by considering two different fault planes shown in (**a**); subset pictures show twin boundary formation for these two cases (this figure is from Reference [109]).

As discussed before, the main issue in utilizing MD simulations to study the MPE alloys, or multicomponent alloys in general, is unavailability of interatomic potentials for these alloys. The accuracy of the results in MD simulations is directly controlled by the interatomic potentials, therefore developing and benchmarking of interatomic potentials for MPE alloys are urgently desired.

As can be seen in Tables 1 and 2, the calculated results for Young's moduli and SFEs show considerable differences with respect to the experimental data. These discrepancies are the results of the configurational disorders of MPE alloys, discussed previously in Section 2 of the current review artilce. SFE results presented in Figure 9 shows how the distribution of atoms in fcc supercells and their relative positions to the stacking fault plane affect the GSFE curves. Although specific modeling

methods, such as SQS have shown good results for some MPE systems, these methods still show large uncertainties for some other MEP alloys, and in general they can be computationally expensive.

Table 2. A summary of available SFE (mJ/m^2) of MPE alloys in literature.

Alloys	$\gamma_{SFE\text{-}DFT}$	$\gamma_{SFE\text{-}MD}$	$\gamma_{SFE\text{-}exp}$
FeCrCoNiMn	21 [111], 27.3 [100], 29.7 [109]	-	25 [117], 26.5 [118], 19 [100]
CoCrFeNi	31.6 [109], 31.7 [100]	-	27 [118]
$CoCrFeNiCu_{0.5}$	29.0 [109]	-	-
CoCrFeNiCu	27.5 [109]	-	-
$CoCrFeNiCuAl_{0.5}$	32.0 [109]	-	-
$CoCrFeNiCuTi_{0.5}$	37.4 [109]	-	-
$CoCrFeNiAl_{0.3}$	35.2 [109]	-	-
CoCrFeNi	31.6 [109]	-	26.8 [117]
$CoCrFeNiCu_{0.5}$	29.0 [109]	-	-
CoCrFeNiCu	27.5 [109]	-	49.0 [115]
$CoCrFeNiCuAl_{0.5}$	32.0 [109]	-	-
$Co_{20}Cr_{26}Fe_{20}Ni_{14}Mn_{20}$	-	-	3.5 [117]
$Co_{15}Cr_{20}Fe_{20}Ni_{25}Mn_{20}$	-	-	38 [118]
$Co_{26}Cr_{18.5}Fe_{18.5}Ni_{18.5}Mn_{18.5}$	-	-	9.7 [100]
$(CoCrFeNi)_{86}Mn_{14}$	-	-	29 [118]
$(CoCrFeNi)_{94}Mn_6$	-	-	28 [118]
FeCrNi	-	20 [114]	-

3.1.3. Solute Strengthening

Solute strengthening is an important characteristic of MPE alloys which causes improvement in the strength of these alloys compared to their constitutes [98]. It is well known that the strength of materials can be changed by adding more solute atoms with large differences in shear moduli and size of solvent and solute atoms [119–121].

First-principles calculations have shown good potential in elucidating the mechanisms of solute strengthening. For instance, the Labusch model was used to study the solute strengthening of fcc NiCoFeCr and NiCoFeCrMn MPE alloys by Varvenne et al. [122]. This model uses dislocation/solute interaction energies from first-principles calculations as inputs, and quantitatively analyzes the effects of composition, strain-rate and temperature on the yield strength and activation volume [122]. Their calculated results for temperature dependent yield strength for $77K \leq T \leq 700K$ showed good agreement with the experimental results available for these MPE alloys [122]. In another study, Varvenne et al. [123] also demonstrated that the additional solute strengthening of MPE alloys due to dilute additions of another solute could be predicted. Moreover, Toda-Caraballo et al. [124,125] applied the Labusch model to compute the hardening parameter in multicomponent alloys, and analyzed the capability of this model in predicting the solid solution hardening (SSH) effect. Wang et al. [80] developed an analytical model based on the Labusch formula to study the effects of the addition of Hf and the resulting lattice distortion on strength and solid solution strengthening mechanisms of bcc $TiNbTaZrHf_x$ MPE alloys. They have predicted that this theoretical model could be used in studying the yield stress, and also in the design of the other bcc MPE alloys.

Besides Labusch model, another general model was proposed by Walbrühl et al. [126] to study the SSH coefficients. Their model is based on an Integrated Computational Materials Engineering (ICME) framework. Different from Labusch [127] models, Walbrühl et al. model directly fits the experimental hardness data, but avoids modeling of misfit parameters. Prediction of SSH of MPE alloys by this model has $\pm 13\%$ overall accuracy [126]. Moreover, I. Toda-Caraballo et al. [128] proposed a methodology which can be employed to compute the distribution of interatomic distances in HEAs by using the unit cell parameter and bulk modulus of component elements. They applied the method for benchmarking the bcc MoNbTaVW alloy and its 5 sub-quaternary systems. The results obtained by this method shows mean variations in the range of 1–2 pm with respect to DFT simulations, which

means it can be used as a better starting point for the time consuming DFT simulations and to quantify the SSH effects in MPE alloys [128].

3.2. Thermo-Chemical Properties

Due to the potential applications in extreme conditions, such as high temperatures or corrosive environments, the studies of thermo-chemical properties of MPE alloys are of great interest.

First-principles approaches were applied to investigate the magnetic and thermal properties of FeCoNiCu-based MPE alloys by Huang et al. [129], and $L1_2$ $(Co,Ni)_3(Al,Mo,Nb)$ phases by Yao et al. [71], providing data for the design of novel tungsten-free high-temperature Co based MPE alloys. In another study and by employing the EMTO-CPA method, Cao et al. [92] predicted that the addition of Al slightly decreased the thermodynamic stability of bcc $Al_xMoNbTiV$ MPE alloys [92]. Furthermore, Löffler et al. [130] assessed the heat capacity of the quaternary AlCuMgSi Q phase precipitation by the combination of experiment and first-principles calculations.

To study the heat-transfer behavior in a WTaMoNb refractory MPE alloy, Zhang et al. [131] developed a macro-grid and micro-grid nested model coupled with the finite difference-finite element (FD-FE) method. They have simulated the thermal stress-strain and temperature distributions in a continuous selective laser melting (SLM) process [131]. Moreover, by coupling finite element model (FEM) with the thermomechanical simulation using Gleeble 3800 thermo-mechanical simulator, Rahul et al. [132] studied the material flow pattern and strain field distribution at different conditions.

Although above efforts have provided some valuable data on thermal or chemical properties of some specific MPE alloys, such data for most of MPE alloys do not exist, and first-principles calculations or MD simulations can be utilized to provide databases for thermal or chemical properties of MPE alloys.

3.3. Magnetic Properties

In addition to the mechanical and thermo-chemical properties of MPE alloys, the magnetic performance of these alloys has attracted great attention from researchers. The magnetic behavior of an MPE alloy depends on the alloying elements and composition, and the crystal structures of the generated phase(s). In recent years, some computational studies, mostly based on DFT calculations, have been conducted to investigate the magnetic properties of some MPE alloys.

For example, a computational method based on DFT calculations and the small unit cell SQS was proposed by Zunger et al. [133] to derive defect formation enthalpies for MPE alloys. This model was designed to simulate the multisite correlation functions and some relevant near neighbor pairs of random substitutional alloys [134]. It was found that the vacancy significantly affects its surrounding local spin magnetic moment. In another study, DFT calculations and five different experimental methods were combined and utilized to determine the magnetic ordering in the CoCrFeMnNi MPE alloys [135]. Their first-principles calculations showed that interactions of Fe-located and/or Mn-located moments with the nearby magnetic structure may be responsible for the experimental macroscopic magnetization bias. Separately, systematic first-principle calculations were carried out in order to study the Curie temperature (T_C) of some equiatomic MPE alloys [136]. An integrated computational study of the mean field, and DFT calculations was also conducted to compute Curie temperatures of MPE alloys [137]. Some candidate MPE alloys with good magnetic properties were revealed, including $CoFeNiCrAg_{0.37}$, $CoFeNiCr_{0.8}Cu_{0.64}$ or $CoFeNiCrAu_{0.29}$. It was also concluded that the hypothetical T_C maps can be directly used in creating ferromagnetic MPE alloys with well-defined target magnetizations and T_C's. Figure 10 shows the calculated local magnetic moments in $Al_xCrMnFeCoNi$ ($0 \leq x \leq 5$) MPE alloys using a first principles approach [138].

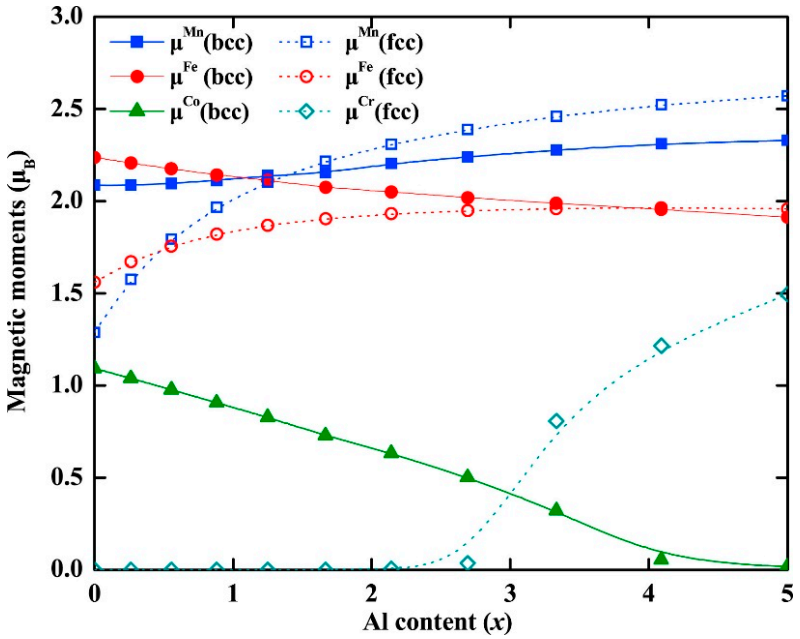

Figure 10. Theoretical local magnetic moments at 0 K for paramagnetic bcc (solid symbols) and fcc (hollowed symbols) $Al_xCrMnFeCoNi$ ($0 \leq x \leq 5$) MPE alloys as a function of Al content (this figure is from Reference [138]).

In some other work, the magnetic properties of CoFeMnNiX (X = Cr, Al, Sn and Ga) MPE alloys were investigated experimentally, and compared with DFT and AIMD simulation results [139,140]. DFT calculations predicted that the anti-ferromagnetic order related to Mn in the CoFeMnNi fcc phase can favor ferromagnetism in the CoFeMnNiAl bcc phase. While CoFeMnNiCr alloy is paramagnetic. By employing DFT calculations and Korringa–Kohn–Rostoker method with the coherent potential approximation (KKR-CPA), Calvo-Dahlborg et al. studied the effects of electronic structures on magnetic properties of some Fe, Co, Cr, and Ni based MPE alloys [141]. Moreover, Sun et al. have studied the dissimilar magnetic moment behaviors of the elements in different concentrations of doped Al in CrMnFeCoNi [138]. Further experimental, theoretical, and computational efforts are still desired in improving the understanding of the magnetic properties of MPE alloys reported in most of these computational studies. Specially to study the effects of grain boundaries and defects on magnetic properties in micro scale, meso-scale models, such as phase-field simulations can be utilized.

4. Summary

In this review article, we have provided a comprehensive overview of current computational modeling and simulation tools for the study and design of MPE alloys. In particular, we focused on the capabilities of different computational modeling tools to study, and predict the structures and properties of MPE alloys. Table 3 summarizes the computational modeling and simulation approaches reported in the literature to study the structures and properties of MPE alloys.

As it can be seen in this table, first-principles approaches have been commonly used to study MPE alloys, and there are many databases created for structures and properties (in particular mechanical properties) of MPE alloys. This can be due to the readiness and the high accuracy of these methods, however the first-principles calculations (e.g., DFT calculations and AIMD simulations) are limited in the model size (up to a few hundred of atoms) and simulation time.

In larger length and time scales, MD simulations were employed in few studies to investigate the structures and mechanical properties of some MPE alloys, but the applicability of such simulations relies on the availability of the interatomic potentials for MPE alloys. The reliability of results is also significantly dependent on the accuracy of interatomic potentials. Therefore, development of

accurate interatomic potentials for MPE alloys is of great interest to study and predict structures and phases of these alloys by MD simulations; such models will also open the door to study nanostructural evolutions in MPE alloys.

To study microstructural evolutions and microstructure-dependent properties of MEP alloys, computational modeling and simulations are needed at the mesoscale (such as PFM simulations). Such studies and models are scarce in the literature, and also for verification and validation of such models high-throughput and in-situ experiments are required.

Table 3. The reviewed computational modeling methods used to study the structures and properties of MPE alloys.

Method		First-Principles	Monte-Carlo	MD	Microscale (e.g., PFM simulations)	FEM	Thermodynamics
Structures/ Phases		a	b	c	×	×	d
Properties	Mechanical	e	×	f	×	g	×
	Thermo-Chemical	h	×	×	×	i	×
	Magnetic	j	×	×	×	×	×

a: [52–65]; b: [74,75] [84,85]; c: [77,78]; d: [17,20,21] [13,22,32–37,39,40,42–45]; e: [87–90,92–95] [106–111] [122–125]; f: [116] [99] [114,115]; g: [105]; h: [71] [92] [129,130]; i: [131,132]; j: [133–141].

Author Contributions: M.B.K., Y.H., and M.A.Z. wrote the manuscript, and M.A.Z. coordinated the whole work.

Conflicts of Interest: The authors state no conflict of interest.

References

1. Miracle, D.; Senkov, O. A critical review of high entropy alloys and related concepts. *Acta Mater.* **2017**, *122*, 448–511. [CrossRef]
2. Murty, B.S.; Yeh, J.-W.; Ranganathan, S. *High-Entropy Alloys*; Butterworth-Heinemann: Oxford, UK, 2014.
3. Zhang, C.; Zhang, F.; Chen, S.; Cao, W. Computational thermodynamics aided high-entropy alloy design. *JOM* **2012**, *64*, 839–845. [CrossRef]
4. Yeh, J.-W. Alloy Design Strategies and Future Trends in High-Entropy Alloys. *JOM* **2013**, *65*, 1759–1771. [CrossRef]
5. Tsai, K.-Y.; Tsai, M.-H.; Yeh, J.-W. Sluggish diffusion in Co–Cr–Fe–Mn–Ni high-entropy alloys. *Acta Mater.* **2013**, *61*, 4887–4897. [CrossRef]
6. Wu, Z.; Parish, C.; Bei, H. Nano-twin mediated plasticity in carbon-containing FeNiCoCrMn high entropy alloys. *J. Alloy. Compd.* **2015**, *647*, 815–822. [CrossRef]
7. Wang, Z.; Baker, I. Interstitial strengthening of a fcc FeNiMnAlCr high entropy alloy. *Mater. Lett.* **2016**, *180*, 153–156. [CrossRef]
8. Li, Z.; Tasan, C.C.; Springer, H.; Gault, B.; Raabe, D. Interstitial atoms enable joint twinning and transformation induced plasticity in strong and ductile high-entropy alloys. *Sci. Rep.* **2017**, *7*, 40704. [CrossRef]
9. Laurent-Brocq, M.; Sauvage, X.; Akhatova, A.; Perrière, L.; Leroy, E.; Champion, Y. Precipitation and Hardness of Carbonitrides in a CrMnFeCoNi High Entropy Alloy. *Adv. Eng. Mater.* **2017**, *19*. [CrossRef]
10. Beyramali Kivy, M.; Kriewall, C.S.; Zaeem, M.A. Formation of chromium-iron carbide by carbon diffusion in Al X CoCrFeNiCu high-entropy alloys. *Mater. Res. Lett.* **2018**, *6*, 321–326. [CrossRef]
11. Fu, X.; Schuh, C.; Olivetti, E. Materials selection considerations for high entropy alloys. *Scr. Mater.* **2017**, *138*, 145–150. [CrossRef]
12. Yeh, J.W.; Chen, S.K.; Lin, S.J.; Gan, J.Y.; Chin, T.S.; Shun, T.T.; Tsau, C.H.; Chang, S.Y. Nanostructured high-entropy alloys with multiple principal elements: Novel alloy design concepts and outcomes. *Adv. Eng. Mater.* **2004**, *6*, 299–303. [CrossRef]
13. Ye, Y.; Wang, Q.; Zhao, Y.; He, Q.; Lu, J.; Yang, Y. Elemental segregation in solid-solution high-entropy alloys: Experiments and modeling. *J. Alloy. Compd.* **2016**, *681*, 167–174. [CrossRef]
14. Zhang, Y.; Yan, X.; Ma, J.; Lu, Z.; Zhao, Y. Compositional gradient films constructed by sputtering in a multicomponent Ti–Al–(Cr, Fe, Ni) system. *J. Mater. Res.* **2018**, *33*, 3330–3338. [CrossRef]

15. Sheng, G.; Liu, C.T. Phase stability in high entropy alloys: Formation of solid-solution phase or amorphous phase. *Prog. Natl. Sci. Mater. Int.* **2011**, *21*, 433–446.
16. Pickering, E.; Jones, N.G. High-entropy alloys: A critical assessment of their founding principles and future prospects. *Int. Mater. Rev.* **2016**, *61*, 183–202. [CrossRef]
17. Zhang, Y.; Zhou, Y.J.; Lin, J.P.; Chen, G.L.; Liaw, P.K. Solid-Solution Phase Formation Rules for Multi-component Alloys. *Adv. Eng. Mater.* **2008**, *10*, 534–538. [CrossRef]
18. Mizutani, U. *The Hume-Rothery Rules for Structurally Complex Alloy Phases, in Surface Properties and Engineering of Complex Intermetallics*; World Scientific: Singapore, 2010; pp. 323–399.
19. Guo, S.; Ng, C.; Lu, J.; Liu, C. Effect of valence electron concentration on stability of fcc or bcc phase in high entropy alloys. *J. Appl. Phys.* **2011**, *109*, 103505. [CrossRef]
20. Tsai, M.-H.; Tsai, K.-Y.; Tsai, C.-W.; Lee, C.; Juan, C.-C.; Yeh, J.-W. Criterion for sigma phase formation in Cr-and V-containing high-entropy alloys. *Mater. Res. Lett.* **2013**, *1*, 207–212. [CrossRef]
21. Tsai, M.-H.; Yeh, J.-W. High-entropy alloys: A critical review. *Mater. Res. Lett.* **2014**, *2*, 107–123. [CrossRef]
22. Morral, J.; Chen, S.-L. High Entropy Alloys, Miscibility Gaps and the Rose Geometry. *J. Phase Equilib. Diffus.* **2017**, *38*, 319–331. [CrossRef]
23. Kaufman, L.; Bernstein, H. *Computer Calculation of Phase Diagrams. With Special Reference to Refractory Metals*; Academic Press: Cambridge, MA, USA, 1970.
24. Kroupa, A. Modelling of phase diagrams and thermodynamic properties using Calphad method—Development of thermodynamic databases. *Comput. Mater. Sci.* **2013**, *66*, 3–13. [CrossRef]
25. Kattner, U.R. The thermodynamic modeling of multicomponent phase equilibria. *JOM* **1997**, *49*, 14–19. [CrossRef]
26. Bale, C.; Bélisle, E.; Chartrand, P.; Decterov, S.; Eriksson, G.; Hack, K.; Jung, I.-H.; Kang, Y.-B.; Melançon, J.; Pelton, A. FactSage thermochemical software and databases—Recent developments. *Calphad* **2009**, *33*, 295–311. [CrossRef]
27. Zhang, Y.; Zhang, J. First principles study of structural and thermodynamic properties of zirconia. *Mater. Today Proc.* **2014**, *1*, 44–54. [CrossRef]
28. Chen, H.-L.; Mao, H.; Chen, Q. Database development and Calphad calculations for high entropy alloys: Challenges, strategies, and tips. *Mater. Chem. Phys.* **2018**, *210*, 279–290. [CrossRef]
29. CompuTherm, L. *Pandat 8.0-Phase Diagram Calculation Software for Multi-Component Systems*; CompuTherm LLC: Madison, WI, USA, 2008; Volume 53719.
30. Idury, K.S.; Murty, B.; Bhatt, J. Thermodynamic modeling and composition design for the formation of Zr–Ti–Cu–Ni–Al high entropy bulk metallic glasses. *Intermetallics* **2015**, *65*, 42–50. [CrossRef]
31. Idury, K.S.; Murty, B.; Bhatt, J. Identifying non-equiatomic high entropy bulk metallic glass formers through thermodynamic approach: A theoretical perspective. *J. Non-Cryst. Solids* **2016**, *450*, 164–173. [CrossRef]
32. Tang, Z.; Gao, M.C.; Diao, H.; Yang, T.; Liu, J.; Zuo, T.; Zhang, Y.; Lu, Z.; Cheng, Y.; Zhang, Y. Aluminum alloying effects on lattice types, microstructures, and mechanical behavior of high-entropy alloys systems. *JOM* **2013**, *65*, 1848–1858. [CrossRef]
33. Sonkusare, R.; Janani, P.D.; Gurao, N.; Sarkar, S.; Sen, S.; Pradeep, K.; Biswas, K. Phase equilibria in equiatomic CoCuFeMnNi high entropy alloy. *Mater. Chem. Phys.* **2018**, *210*, 269–278. [CrossRef]
34. Saal, J.E.; Berglund, I.S.; Sebastian, J.T.; Liaw, P.K.; Olson, G.B. Equilibrium high entropy alloy phase stability from experiments and thermodynamic modeling. *Scr. Mater.* **2018**, *146*, 5–8. [CrossRef]
35. Yao, H.; Qiao, J.; Gao, M.; Hawk, J.; Ma, S.; Zhou, H.; Zhang, Y. NbTaV-(Ti, W) refractory high-entropy alloys: Experiments and modeling. *Mater. Sci. Eng. A* **2016**, *674*, 203–211. [CrossRef]
36. Feng, R.; Gao, M.C.; Lee, C.; Mathes, M.; Zuo, T.; Chen, S.; Hawk, J.A.; Zhang, Y.; Liaw, P.K. Design of light-weight high-entropy alloys. *Entropy* **2016**, *18*, 333. [CrossRef]
37. Stepanov, N.; Yurchenko, N.Y.; Skibin, D.; Tikhonovsky, M.; Salishchev, G. Structure and mechanical properties of the AlCrxNbTiV (x = 0, 0.5, 1, 1.5) high entropy alloys. *J. Alloy. Compd.* **2015**, *652*, 266–280. [CrossRef]
38. Gwalani, B.; Gorsse, S.; Choudhuri, D.; Styles, M.; Zheng, Y.; Mishra, R.S.; Banerjee, R. Modifying transformation pathways in high entropy alloys or complex concentrated alloys via thermo-mechanical processing. *Acta Mater.* **2018**, *153*, 169–185. [CrossRef]
39. Abu-Odeh, A.; Galvan, E.; Kirk, T.; Mao, H.; Chen, Q.; Mason, P.; Malak, R.; Arróyave, R. Efficient exploration of the High Entropy Alloy composition-phase space. *Acta Mater.* **2018**. [CrossRef]

40. Tancret, F.; Toda-Caraballo, I.; Menou, E.; Díaz-Del, P.E.J.R. Designing high entropy alloys employing thermodynamics and Gaussian process statistical analysis. *Mater. Des.* **2017**, *115*, 486–497. [CrossRef]
41. Gorsse, S.; Tancret, F. Current and emerging practices of CALPHAD toward the development of high entropy alloys and complex concentrated alloys. *J. Mater. Res.* **2018**, *33*, 2899–2923. [CrossRef]
42. Liu, Y.; Ma, S.; Gao, M.C.; Zhang, C.; Zhang, T.; Yang, H.; Wang, Z.; Qiao, J. Tribological properties of AlCrCuFeNi2 high-entropy alloy in different conditions. *Metall. Mater. Trans. A* **2016**, *47*, 3312–3321. [CrossRef]
43. Haase, C.; Tang, F.; Wilms, M.B.; Weisheit, A.; Hallstedt, B. Combining thermodynamic modeling and 3D printing of elemental powder blends for high-throughput investigation of high-entropy alloys–Towards rapid alloy screening and design. *Mater. Sci. Eng. A* **2017**, *688*, 180–189. [CrossRef]
44. Arslan, H.; Dogan, A. Thermodynamic investigations on the component dependences of high-entropy alloys. *Russ. J. Phys. Chem. A* **2016**, *90*, 2339–2345. [CrossRef]
45. Eshed, E.; Larianovsky, N.; Kovalevsky, A.; Popov, V., Jr.; Gorbachev, I.; Popov, V.; Katz-Demyanetz, A. Microstructural Evolution and Phase Formation in 2nd-Generation Refractory-Based High Entropy Alloys. *Materials* **2018**, *11*, 175. [CrossRef] [PubMed]
46. Beyramali Kivy, M.; Zaeem, M.A.; Lekakh, S. Investigating phase formations in cast AlFeCoNiCu high entropy alloys by combination of computational modeling and experiments. *Mater. Des.* **2017**, *127*, 224–232. [CrossRef]
47. Toda-Caraballo, I.; Wróbel, J.; Nguyen-Manh, D.; Perez, P.; Rivera-Díaz-del-Castillo, P. Simulation and modeling in high entropy alloys. *JOM* **2017**, *69*, 2137–2149. [CrossRef]
48. Kresse, G.; Marsman, O.; Furthmuller, J. VASP the Guide. Available online: http://cms.mpi.univie.ac.at/vasp/vasp.pdf (accessed on 24 April 2016).
49. Giannozzi, P.; Baroni, S.; Bonini, N.; Calandra, M.; Car, R.; Cavazzoni, C.; Ceresoli, D.; Chiarotti, G.L.; Cococcioni, M.; Dabo, I. QUANTUM ESPRESSO: A modular and open-source software project for quantum simulations of materials. *J. Phys. Condens. Matter* **2009**, *21*, 395502. [CrossRef] [PubMed]
50. Gonze, X.; Beuken, J.-M.; Caracas, R.; Detraux, F.; Fuchs, M.; Rignanese, G.-M.; Sindic, L.; Verstraete, M.; Zerah, G.; Jollet, F. First-principles computation of material properties: The ABINIT software project. *Comput. Mater. Sci.* **2002**, *25*, 478–492. [CrossRef]
51. Segall, M.; Lindan, P.J.; Probert, M.A.; Pickard, C.J.; Hasnip, P.J.; Clark, S.; Payne, M. First-principles simulation: Ideas, illustrations and the CASTEP code. *J. Phys. Condens. Matter* **2002**, *14*, 2717. [CrossRef]
52. Ma, D.; Grabowski, B.; Körmann, F.; Neugebauer, J.; Raabe, D. Ab initio thermodynamics of the CoCrFeMnNi high entropy alloy: Importance of entropy contributions beyond the configurational one. *Acta Mater.* **2015**, *100*, 90–97. [CrossRef]
53. Niu, C.; Zaddach, A.; Koch, C.; Irving, D. First principles exploration of near-equiatomic NiFeCrCo high entropy alloys. *J. Alloy. Compd.* **2016**, *672*, 510–520. [CrossRef]
54. Yalamanchili, K.; Wang, F.; Schramm, I.; Andersson, J.; Jöesaar, M.J.; Tasnadi, F.; Muecklich, F.; Ghafoor, N.; Odén, M. Exploring the high entropy alloy concept in (AlTiVNbCr) N. *Thin Solid Films* **2017**, *636*, 346–352. [CrossRef]
55. Jiang, C.; Uberuaga, B.P. Efficient ab initio modeling of random multicomponent alloys. *Phys. Rev. Lett.* **2016**, *116*, 105501. [CrossRef]
56. Tian, F.; Varga, L.K.; Vitos, L. Predicting single phase CrMoWX high entropy alloys from empirical relations in combination with first-principles calculations. *Intermetallics* **2017**, *83*, 9–16. [CrossRef]
57. Li, Z.; Körmann, F.; Grabowski, B.; Neugebauer, J.; Raabe, D. Ab initio assisted design of quinary dual-phase high-entropy alloys with transformation-induced plasticity. *Acta Mater.* **2017**, *136*, 262–270. [CrossRef]
58. Heidelmann, M.; Feuerbacher, M.; Ma, D.; Grabowski, B. Structural anomaly in the high-entropy alloy ZrNbTiTaHf. *Intermetallics* **2016**, *68*, 11–15. [CrossRef]
59. Mu, Y.; Liu, H.; Liu, Y.; Zhang, X.; Jiang, Y.; Dong, T. An ab initio and experimental studies of the structure, mechanical parameters and state density on the refractory high-entropy alloy systems. *J. Alloy. Compd.* **2017**, *714*, 668–680. [CrossRef]
60. Zhang, F.; Zhao, S.; Jin, K.; Bei, H.; Popov, D.; Park, C.; Neuefeind, J.C.; Weber, W.J.; Zhang, Y. Pressure-induced fcc to hcp phase transition in Ni-based high entropy solid solution alloys. *Appl. Phys. Lett.* **2017**, *110*, 011902. [CrossRef]

61. Tian, F.; Delczeg, L.; Chen, N.; Varga, L.K.; Shen, J.; Vitos, L. Structural stability of NiCoFeCrAl x high-entropy alloy from ab initio theory. *Phys. Rev. B* **2013**, *88*, 085128. [CrossRef]
62. Middleburgh, S.; King, D.; Lumpkin, G.; Cortie, M.; Edwards, L. Segregation and migration of species in the CrCoFeNi high entropy alloy. *J. Alloy. Compd.* **2014**, *599*, 179–182. [CrossRef]
63. Takaki, T.; Ohno, M.; Shibuta, Y.; Sakane, S.; Shimokawabe, T.; Aoki, T. Two-dimensional phase-field study of competitive grain growth during directional solidification of polycrystalline binary alloy. *J. Cryst. Growth* **2016**, *442*, 14–24. [CrossRef]
64. Leong, Z.; Wróbel, J.S.; Dudarev, S.L.; Goodall, R.; Todd, I.; Nguyen-Manh, D. The effect of electronic structure on the phases present in high entropy alloys. *Sci. Rep.* **2017**, *7*, 39803. [CrossRef] [PubMed]
65. Gutierrez, M.; Rodriguez, G.; Bozzolo, G.; Mosca, H. Melting temperature of CoCrFeNiMn high-entropy alloys. *Comput. Mater. Sci.* **2018**, *148*, 69–75. [CrossRef]
66. Zhang, Y.; Stocks, G.M.; Jin, K.; Lu, C.; Bei, H.; Sales, B.C.; Wang, L.; Béland, L.K.; Stoller, R.E.; Samolyuk, G.D. Influence of chemical disorder on energy dissipation and defect evolution in concentrated solid solution alloys. *Nat. Commun.* **2015**, *6*, 8736. [CrossRef] [PubMed]
67. Pielnhofer, F.; Schöneich, M.; Lorenz, T.; Yan, W.; Nilges, T.; Weihrich, R.; Schmidt, P. A Rational Approach to IrPTe–DFT and CalPhaD Studies on Phase Stability, Formation, and Structure of IrPTe. *Z. Anorg. Allg. Chem.* **2015**, *641*, 1099–1105. [CrossRef]
68. Mathieu, R.; Dupin, N.; Crivello, J.-C.; Yaqoob, K.; Breidi, A.; Fiorani, J.-M.; David, N.; Joubert, J.-M. CALPHAD description of the Mo–Re system focused on the sigma phase modeling. *Calphad* **2013**, *43*, 18–31. [CrossRef]
69. Bigdeli, S. *Developing the Third Generation of Calphad Databases: What Can ab-Initio Contribute?* KTH Royal Institute of Technology: Stockholm, Sweden, 2017.
70. Ikeda, Y.; Grabowski, B.; Körmann, F. Ab initio phase stabilities and mechanical properties of multicomponent alloys: A comprehensive review for high entropy alloys and compositionally complex alloys. *Mater. Charact.* **2018**, *147*, 464–511. [CrossRef]
71. Yao, Q.; Shang, S.-L.; Wang, K.; Liu, F.; Wang, Y.; Wang, Q.; Lu, T.; Liu, Z.-K. Phase stability, elastic, and thermodynamic properties of the L1 2 (Co, Ni) 3 (Al, Mo, Nb) phase from first-principles calculations. *J. Mater. Res.* **2017**, *32*, 2100–2108. [CrossRef]
72. Gao, M.C.; Zhang, B.; Guo, S.; Qiao, J.; Hawk, J. High-entropy alloys in hexagonal close-packed structure. *Metall. Mater. Trans. A* **2016**, *47*, 3322–3332. [CrossRef]
73. Gao, M.C.; Zhang, B.; Yang, S.; Guo, S. Senary refractory high-entropy alloy HfNbTaTiVZr. *Metall. Mater. Trans. A* **2016**, *47*, 3333–3345. [CrossRef]
74. Choi, W.-M.; Jo, Y.H.; Sohn, S.S.; Lee, S.; Lee, B.-J. Understanding the physical metallurgy of the CoCrFeMnNi high-entropy alloy: An atomistic simulation study. *npj Comput. Mater.* **2018**, *4*, 1. [CrossRef]
75. Sharma, A.; Deshmukh, S.A.; Liaw, P.K.; Balasubramanian, G. Crystallization kinetics in AlxCrCoFeNi ($0 \leq x \leq 40$) high-entropy alloys. *Scr. Mater.* **2017**, *141*, 54–57. [CrossRef]
76. Mooney, C.Z. *Monte Carlo Simulation*; Sage Publications: Thousand Oaks, CA, USA, 1997; Volume 116.
77. Anzorena, M.S.; Bertolo, A.; Gagetti, L.; Kreiner, A.; Mosca, H.; Bozzolo, G.; del Grosso, M. Characterization and modeling of a MoTaVWZr high entropy alloy. *Mater. Des.* **2016**, *111*, 382–388. [CrossRef]
78. Feng, W.Q.; Zheng, S.M.; Qi, Y.; Wang, S.Q. Periodic Maximum Entropy Random Structure Models for High-Entropy Alloys. *Mater. Sci. Forum* **2017**, *898*, 611–621. [CrossRef]
79. Widom, M. Modeling the structure and thermodynamics of high-entropy alloys. *J. Mater. Res.* **2018**, *33*, 2881–2898. [CrossRef]
80. Wang, Z.; Fang, Q.; Li, J.; Liu, B.; Liu, Y. Effect of lattice distortion on solid solution strengthening of BCC high-entropy alloys. *J. Mater. Sci. Technol.* **2018**, *34*, 349–354. [CrossRef]
81. del Grosso, M.; Bozzolo, G.; Mosca, H. Modeling of high entropy alloys of refractory elements. *Phys. B Condens. Matter* **2012**, *407*, 3285–3287. [CrossRef]
82. Toda-Caraballo, I.; Rivera-Díaz-del-Castillo, P.E. Modelling and design of magnesium and high entropy alloys through combining statistical and physical models. *JOM* **2015**, *67*, 108–117. [CrossRef]
83. Kucza, W.; Dąbrowa, J.; Cieślak, G.; Berent, K.; Kulik, T.; Danielewski, M. Studies of "sluggish diffusion" effect in Co-Cr-Fe-Mn-Ni, Co-Cr-Fe-Ni and Co-Fe-Mn-Ni high entropy alloys; determination of tracer diffusivities by combinatorial approach. *J. Alloy. Compd.* **2018**, *731*, 920–928. [CrossRef]

84. Fernández-Caballero, A.; Fedorov, M.; Wróbel, J.S.; Mummery, P.M.; Nguyen-Manh, D. Configurational Entropy in Multicomponent Alloys: Matrix Formulation from Ab Initio Based Hamiltonian and Application to the FCC Cr-Fe-Mn-Ni System. *Entropy* **2019**, *21*, 68. [CrossRef]
85. Fernandez-Caballero, A.; Wróbel, J.; Mummery, P.; Nguyen-Manh, D. Short-range order in high entropy alloys: Theoretical formulation and application to Mo-Nb-Ta-VW system. *J. Phase Equilib. Diffus.* **2017**, *38*, 391–403. [CrossRef]
86. Gludovatz, B.; Hohenwarter, A.; Catoor, D.; Chang, E.H.; George, E.P.; Ritchie, R.O. A fracture-resistant high-entropy alloy for cryogenic applications. *Science* **2014**, *345*, 1153–1158. [CrossRef]
87. Andersen, O.; Jepsen, O.; Krier, G. Exact Muffin-Tin Orbital Theory. In *Lectures on Methods of Electronic Structure Calculations*; World Scientific: Singapore, 1994; pp. 63–124.
88. Vitos, L.; Skriver, H.L.; Johansson, B.; Kollár, J. Application of the exact muffin-tin orbitals theory: The spherical cell approximation. *Comput. Mater. Sci.* **2000**, *18*, 24–38. [CrossRef]
89. Tian, F.; Varga, L.K.; Shen, J.; Vitos, L. Calculating elastic constants in high-entropy alloys using the coherent potential approximation: Current issues and errors. *Comput. Mater. Sci.* **2016**, *111*, 350–358. [CrossRef]
90. Tian, F.; Varga, L.K.; Chen, N.; Shen, J.; Vitos, L. Ab initio design of elastically isotropic TiZrNbMoVx high-entropy alloys. *J. Alloy. Compd.* **2014**, *599*, 19–25. [CrossRef]
91. Li, X.; Irving, D.L.; Vitos, L. First-principles investigation of the micromechanical properties of fcc-hcp polymorphic high-entropy alloys. *Sci. Rep.* **2018**, *8*, 11196. [CrossRef] [PubMed]
92. Cao, P.; Ni, X.; Tian, F.; Varga, L.K.; Vitos, L. Ab initio study of AlxMoNbTiV high-entropy alloys. *J. Phys. Condens. Matter* **2015**, *27*, 075401. [CrossRef] [PubMed]
93. Li, X.; Tian, F.; Schönecker, S.; Zhao, J.; Vitos, L. Ab initio-predicted micro-mechanical performance of refractory high-entropy alloys. *Sci. Rep.* **2015**, *5*, 12334. [CrossRef] [PubMed]
94. Li, X.; Schönecker, S.; Li, W.; Varga, L.K.; Irving, D.L.; Vitos, L. Tensile and shear loading of four fcc high-entropy alloys: A first-principles study. *Phys. Rev. B* **2018**, *97*, 094102. [CrossRef]
95. Ge, H.; Song, H.; Shen, J.; Tian, F. Effect of alloying on the thermal-elastic properties of 3d high-entropy alloys. *Mater. Chem. Phys.* **2018**, *210*, 320–326. [CrossRef]
96. Zheng, S.-M.; Feng, W.-Q.; Wang, S.-Q. Elastic properties of high entropy alloys by MaxEnt approach. *Comput. Mater. Sci.* **2018**, *142*, 332–337. [CrossRef]
97. Tian, F.; Wang, D.; Shen, J.; Wang, Y. An ab initio investgation of ideal tensile and shear strength of TiVNbMo high-entropy alloy. *Mater. Lett.* **2016**, *166*, 271–275. [CrossRef]
98. Qiu, S.; Miao, N.; Zhou, J.; Guo, Z.; Sun, Z. Strengthening mechanism of aluminum on elastic properties of NbVTiZr high-entropy alloys. *Intermetallics* **2018**, *92*, 7–14. [CrossRef]
99. Sharma, A.; Balasubramanian, G. Dislocation dynamics in Al0. 1CoCrFeNi high-entropy alloy under tensile loading. *Intermetallics* **2017**, *91*, 31–34. [CrossRef]
100. Zaddach, A.; Niu, C.; Koch, C.; Irving, D. Mechanical properties and stacking fault energies of NiFeCrCoMn high-entropy alloy. *JOM* **2013**, *65*, 1780–1789. [CrossRef]
101. Senkov, O.; Miller, J.; Miracle, D.; Woodward, C. Accelerated exploration of multi-principal element alloys with solid solution phases. *Nat. Commun.* **2015**, *6*, 6529. [CrossRef] [PubMed]
102. Lucas, M.; Belyea, D.; Bauer, C.; Bryant, N.; Michel, E.; Turgut, Z.; Leontsev, S.; Horwath, J.; Semiatin, S.; McHenry, M. Thermomagnetic analysis of FeCoCr x Ni alloys: Magnetic entropy of high-entropy alloys. *J. Appl. Phys.* **2013**, *113*, 17A923. [CrossRef]
103. Dirras, G.; Lilensten, L.; Djemia, P.; Laurent-Brocq, M.; Tingaud, D.; Couzinié, J.-P.; Perrière, L.; Chauveau, T.; Guillot, I. Elastic and plastic properties of as-cast equimolar TiHfZrTaNb high-entropy alloy. *Mater. Sci. Eng. A* **2016**, *654*, 30–38. [CrossRef]
104. Dirras, G.; Gubicza, J.; Heczel, A.; Lilensten, L.; Couzinié, J.-P.; Perrière, L.; Guillot, I.; Hocini, A. Microstructural investigation of plastically deformed Ti20Zr20Hf20Nb20Ta20 high entropy alloy by X-ray diffraction and transmission electron microscopy. *Mater. Charact.* **2015**, *108*, 1–7. [CrossRef]
105. Štamborská, M.; Lapin, J. Effect of anisotropic microstructure on high-temperature compression deformation of CoCrFeNi based complex concentrated alloy. *Kov. Mater.* **2017**, *55*, 369–378.
106. Lu, Y.; Dong, Y.; Jiang, L.; Wang, T.; Li, T.; Zhang, Y. A criterion for topological close-packed phase formation in high entropy alloys. *Entropy* **2015**, *17*, 2355–2366. [CrossRef]
107. Ye, Y.; Zhang, Y.; He, Q.; Zhuang, Y.; Wang, S.; Shi, S.; Hu, A.; Fan, J.; Yang, Y. Atomic-scale distorted lattice in chemically disordered equimolar complex alloys. *Acta Mater.* **2018**, *150*, 182–194. [CrossRef]

108. Ye, Y.; Liu, C.; Yang, Y. A geometric model for intrinsic residual strain and phase stability in high entropy alloys. *Acta Mater.* **2015**, *94*, 152–161. [CrossRef]
109. Kivy, M.B.; Asle Zaeem, M. Generalized stacking fault energies, ductilities, and twinnabilities of CoCrFeNi-based face-centered cubic high entropy alloys. *Scr. Mater.* **2017**, *139*, 83–86. [CrossRef]
110. Zhao, S.; Stocks, G.M.; Zhang, Y. Stacking fault energies of face-centered cubic concentrated solid solution alloys. *Acta Mater.* **2017**, *134*, 334–345. [CrossRef]
111. Huang, S.; Li, W.; Lu, S.; Tian, F.; Shen, J.; Holmström, E.; Vitos, L. Temperature dependent stacking fault energy of FeCrCoNiMn high entropy alloy. *Scr. Mater.* **2015**, *108*, 44–47. [CrossRef]
112. Pei, Z.; Eisenbach, M. Acceleration of the Particle Swarm Optimization for Peierls–Nabarro modeling of dislocations in conventional and high-entropy alloys. *Comput. Phys. Commun.* **2017**, *215*, 7–12. [CrossRef]
113. Choudhuri, D.; Gwalani, B.; Gorsse, S.; Komarasamy, M.; Mantri, S.A.; Srinivasan, S.G.; Mishra, R.S.; Banerjee, R. Enhancing strength and strain hardenability via deformation twinning in fcc-based high entropy alloys reinforced with intermetallic compounds. *Acta Mater.* **2019**, *165*, 420–430. [CrossRef]
114. Wang, Z.; Li, J.; Fang, Q.; Liu, B.; Zhang, L. Investigation into nanoscratching mechanical response of AlCrCuFeNi high-entropy alloys using atomic simulations. *Appl. Surf. Sci.* **2017**, *416*, 470–481. [CrossRef]
115. Li, J.; Fang, Q.; Liu, B.; Liu, Y. Transformation induced softening and plasticity in high entropy alloys. *Acta Mater.* **2018**, *147*, 35–41. [CrossRef]
116. Smith, T.; Hooshmand, M.; Esser, B.; Otto, F.; McComb, D.; George, E.; Ghazisaeidi, M.; Mills, M. Atomic-scale characterization and modeling of 60 dislocations in a high-entropy alloy. *Acta Mater.* **2016**, *110*, 352–363. [CrossRef]
117. Zaddach, A.; Scattergood, R.; Koch, C. Tensile properties of low-stacking fault energy high-entropy alloys. *Mater. Sci. Eng. A* **2015**, *636*, 373–378. [CrossRef]
118. Liu, S.; Wu, Y.; Wang, H.; He, J.; Liu, J.; Chen, C.; Liu, X.; Wang, H.; Lu, Z. Stacking fault energy of face-centered-cubic high entropy alloys. *Intermetallics* **2018**, *93*, 269–273. [CrossRef]
119. Ventelon, L.; Lüthi, B.; Clouet, E.; Proville, L.; Legrand, B.; Rodney, D.; Willaime, F. Dislocation core reconstruction induced by carbon segregation in bcc iron. *Phys. Rev. B* **2015**, *91*, 220102. [CrossRef]
120. Tsuru, T.; Chrzan, D. Effect of solute atoms on dislocation motion in Mg: An electronic structure perspective. *Sci. Rep.* **2015**, *5*, 8793. [CrossRef] [PubMed]
121. Yu, Q.; Qi, L.; Tsuru, T.; Traylor, R.; Rugg, D.; Morris, J.; Asta, M.; Chrzan, D.; Minor, A.M. Origin of dramatic oxygen solute strengthening effect in titanium. *Science* **2015**, *347*, 635–639. [CrossRef] [PubMed]
122. Varvenne, C.; Leyson, G.; Ghazisaeidi, M.; Curtin, W. Solute strengthening in random alloys. *Acta Mater.* **2017**, *124*, 660–683. [CrossRef]
123. Varvenne, C.; Curtin, W.A. Strengthening of high entropy alloys by dilute solute additions: CoCrFeNiAlx and CoCrFeNiMnAlx alloys. *Scr. Mater.* **2017**, *138*, 92–95. [CrossRef]
124. Toda-Caraballo, I.; Rivera-Díaz-del-Castillo, P.E. Modelling solid solution hardening in high entropy alloys. *Acta Mater.* **2015**, *85*, 14–23. [CrossRef]
125. Toda-Caraballo, I. A general formulation for solid solution hardening effect in multicomponent alloys. *Scr. Mater.* **2017**, *127*, 113–117. [CrossRef]
126. Walbrühl, M.; Linder, D.; Ågren, J.; Borgenstam, A. Modelling of solid solution strengthening in multicomponent alloys. *Mater. Sci. Eng. A* **2017**, *700*, 301–311. [CrossRef]
127. Labusch, R. A statistical theory of solid solution hardening. *Phys. Status Solidi* **1970**, *41*, 659–669. [CrossRef]
128. Toda-Caraballo, I.; Wróbel, J.; Dudarev, S.; Nguyen-Manh, D.; Rivera-Díaz-del-Castillo, P. Interatomic spacing distribution in multicomponent alloys. *Acta Mater.* **2015**, *97*, 156–169. [CrossRef]
129. Huang, S.; Vida, Á.; Heczel, A.; Holmström, E.; Vitos, L. Thermal Expansion, Elastic and Magnetic Properties of FeCoNiCu-Based High-Entropy Alloys Using First-Principle Theory. *JOM* **2017**, *69*, 2107–2112. [CrossRef]
130. Löffler, A.; Zendegani, A.; Gröbner, J.; Hampl, M.; Schmid-Fetzer, R.; Engelhardt, H.; Rettenmayr, M.; Körmann, F.; Hickel, T.; Neugebauer, J. Quaternary Al-Cu-Mg-Si Q Phase: Sample Preparation, Heat Capacity Measurement and First-Principles Calculations. *J. Phase Equilib. Diffus.* **2016**, *37*, 119–126. [CrossRef]
131. Zhang, H.; Xu, W.; Xu, Y.; Lu, Z.; Li, D. The thermal-mechanical behavior of WTaMoNb high-entropy alloy via selective laser melting (SLM): Experiment and simulation. *Int. J. Adv. Manuf. Technol.* **2018**, *96*, 461–474. [CrossRef]

132. Rahul, M.; Samal, S.; Venugopal, S.; Phanikumar, G. Experimental and finite element simulation studies on hot deformation behaviour of AlCoCrFeNi2. 1 eutectic high entropy alloy. *J. Alloy. Compd.* **2018**, *749*, 1115–1127. [CrossRef]
133. Zunger, A.; Wei, S.-H.; Ferreira, L.; Bernard, J.E. Special quasirandom structures. *Phys. Rev. Lett.* **1990**, *65*, 353. [CrossRef] [PubMed]
134. Chen, W.; Ding, X.; Feng, Y.; Liu, X.; Liu, K.; Lu, Z.; Li, D.; Li, Y.; Liu, C.; Chen, X.-Q. Vacancy formation enthalpies of high-entropy FeCoCrNi alloy via first-principles calculations and possible implications to its superior radiation tolerance. *J. Mater. Sci. Technol.* **2018**, *34*, 355–364. [CrossRef]
135. Schneeweiss, O.; Friák, M.; Dudová, M.; Holec, D.; Šob, M.; Kriegner, D.; Holý, V.; Beran, P.; George, E.P.; Neugebauer, J. Magnetic properties of the CrMnFeCoNi high-entropy alloy. *Phys. Rev. B* **2017**, *96*, 014437. [CrossRef]
136. Huang, S.; Holmström, E.; Eriksson, O.; Vitos, L. Mapping the magnetic transition temperatures for medium-and high-entropy alloys. *Intermetallics* **2018**, *95*, 80–84. [CrossRef]
137. Körmann, F.; Ma, D.; Belyea, D.D.; Lucas, M.S.; Miller, C.W.; Grabowski, B.; Sluiter, M.H. "Treasure maps" for magnetic high-entropy-alloys from theory and experiment. *Appl. Phys. Lett.* **2015**, *107*, 142404. [CrossRef]
138. Sun, X.; Zhang, H.; Lu, S.; Ding, X.; Wang, Y.; Vitos, L. Phase selection rule for Al-doped CrMnFeCoNi high-entropy alloys from first-principles. *Acta Mater.* **2017**, *140*, 366–374. [CrossRef]
139. Ma, S.; Zhang, S.; Gao, M.; Liaw, P.; Zhang, Y. A Successful Synthesis of the CoCrFeNiAl0. 3 Single-Crystal, High-Entropy Alloy by Bridgman Solidification. *JOM* **2013**, *65*, 1751–1758. [CrossRef]
140. Zuo, T.; Gao, M.C.; Ouyang, L.; Yang, X.; Cheng, Y.; Feng, R.; Chen, S.; Liaw, P.K.; Hawk, J.A.; Zhang, Y. Tailoring magnetic behavior of CoFeMnNiX (X = Al, Cr, Ga, and Sn) high entropy alloys by metal doping. *Acta Mater.* **2017**, *130*, 10–18. [CrossRef]
141. Calvo-Dahlborg, M.; Cornide, J.; Tobola, J.; Nguyen-Manh, D.; Wróbel, J.; Juraszek, J.; Jouen, S.; Dahlborg, U. Interplay of electronic, structural and magnetic properties as the driving feature of high-entropy CoCrFeNiPd alloys. *J. Phys. D Appl. Phys.* **2017**, *50*, 185002. [CrossRef]